State Trajectory Generation of MIMO Multirate Feedforward for Perfect Tracking Control in High-Precision Stage

Masahiro Mae and Hiroshi Fujimoto
The University of Tokyo
5-1-5, Kashiwanoha, Kashiwa, Chiba, 277-8561, Japan
Phone: +81-4-7136-3881
Email: mmae@ieee.org, fujimoto@k.u-tokyo.ac.jp

***Abstract*—Multirate feedforward control is widely used for the control of precise systems such as the high-precision stages and the hard disk drives. In the multirate feedforward control, it is possible to obtain a control input that achieves perfect tracking for the state trajectory. Therefore, it is necessary to generate a state trajectory corresponding to the output trajectory in advance. In this paper, the authors propose a state trajectory generation from an output trajectory for a multi-input multi-output system using singular value decomposition. The effectiveness of this method is verified through simulation and experiments.**

***Index Terms*—singular value decomposition, state trajectory generation, multirate feedforward control, perfect tracking control, multi-input multi-output system, high-precision stage**

I. Introduction

Multirate feedforward control is widely used for the control of the precise systems such as the high precision stages and the hard disk drives. Multirate feedforward solves the problem of discretize unstable zeros in the discrete system and achieves perfect tracking control (PTC) [1]. The word "perfect tracking control (PTC)" is defined as "the plant output perfectly tracks the desired trajectory with zero tracking error at every sampling point" [2].

The high-precision stages have an important role in the manufacturing of semiconductors and liquid crystal panels [3]. Multirate feedforward control is commonly applied to the high-precision stages. The high-performance demand of semiconductors and liquid crystal panels is increasing year by year in the world [4]. The conventional high-precision stages are single-input single-output (SISO) 1 degree of freedom (DOF) systems mechanically constrained other than long stroke. However, in recent years, from the demands of further precision, the high-precision stages become 6 DOF systems which are floating by air bearings without mechanical frictions, and they are attempted to be controlled as multi-input multi-output (MIMO) systems [5]. In MIMO systems represented by 6 DOF system, the coupling of each DOF is one of the problems for the high-precision control [6]. For coupled MIMO systems, it is common to use a precompensator to decouple and then control by using SISO controllers, but the precompensator is not considering the discretize unstable zero problems. Therefore, in order to achieve perfect tracking control, the multirate feedforward controller for MIMO systems is needed to be designed. In multirate feedforward control for MIMO systems, the design of the controller is not unique depending on the select the $\boldsymbol{B}$ matrix from the generalizable controllability indices, and several kinds of controllers are designed [7]. Using multirate feedforward control for MIMO systems, PTC can be achieved in several patterns [8].

In the multirate feedforward control, it is possible to obtain a control input for achieving the perfect tracking control for the state trajectory. Therefore, it is necessary to calculate the state trajectory corresponding to the output trajectory in advance. In the conventional multirate feedforward control for the SISO system, the state trajectory corresponding to the output trajectory is calculated by convolving the output equation of the controllable canonical form in the time domain. If the system has the unstable zeros in the continuous time domain, it is not possible to directly calculate the stable inverse system. In this case, the preactuation perfect tracking control (PPTC) using time axis reversal [9] or the stable inversion [10] have been used. On the other hand, in the multirate feedforward control for the MIMO system, it is difficult to calculate the state trajectory corresponding to the output trajectory because of the presence of off-diagonal terms in the $\boldsymbol{C}$ matrix of the output equation, and the complexity of the controllable canonical form in MIMO systems.

In this paper, the authors propose the method to generate the state trajectory corresponding to the output trajectory for multirate feedforward control in MIMO system using singular value decomposition (SVD). The authors control the high-precision stage with 6 DOF, and consider 2DOF system with the translation along the x axis and the pitching around the y axis. The authors propose the method of state trajectory generation using singular value decomposition and the multirate feedforward controller design in the MIMO system, and the effectiveness of the proposed method compared with the conventional method is verified through the simulation and the experiment.

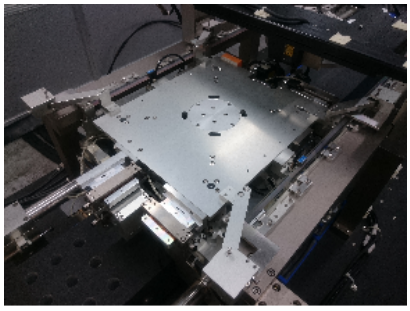

(a) Photograph of the 6-DOF high-precision stage.

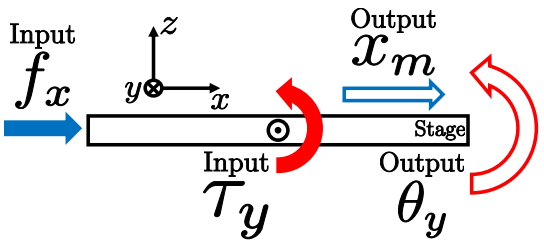

(b) Coupling problem between x and θ_y.

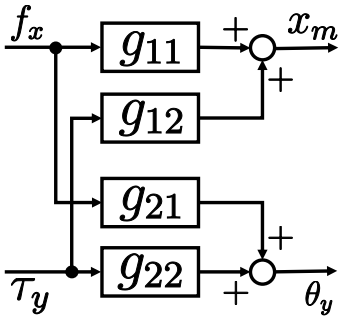

(c) Block diagram of the plant.

Fig. 1. Details of the plant.

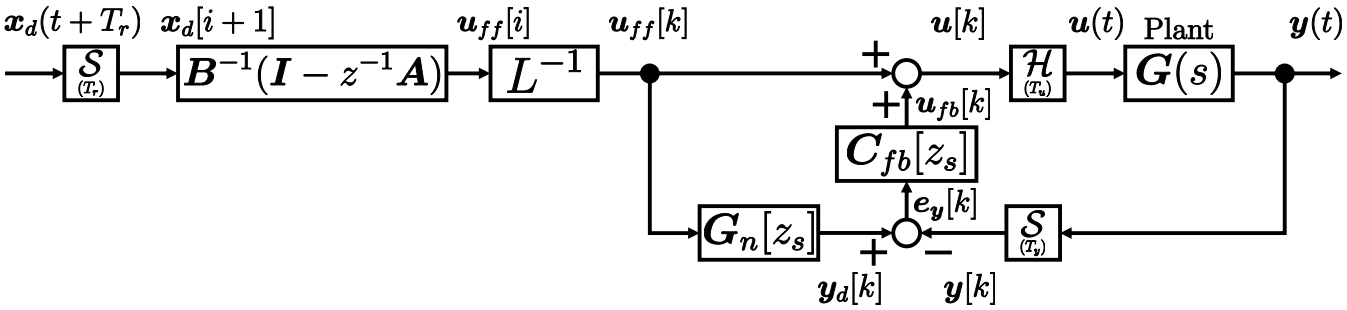

Fig. 2. Block diagram of the controller with the plant which does not have unstable intrinsic zeros. $\mathcal{S}$, $\mathcal{H}$, and L denote a sampler, holder, and lifting operator [11], respectively, z and z_s denote e^{sT_r} and e^{sT_u}, respectively.

II. Controller Design

A. State Trajectory Generaion

In this paper, the authors think about the plant without the continuous unstable zeros.

1) State Trajectory Generation for Single-Input Single-Output System: The conventional method of generating a state trajectory from an output trajectory in the SISO system will be described below.

The transfer function of the plant is given by

$$P(s) = \frac{B(s)}{A(s)} = \frac{b_m s^m + b_{m-1}s^{m-1} + \cdots + b_0}{s^n + a_{n-1}s^{n-1} + \cdots + a_0} \tag{1}$$

The state space representation of this plant in controllable canonical form is given by

$$\frac{\mathrm{d}}{\mathrm{d}t}\begin{bmatrix} x_1(t) \\ x_2(t) \\ \vdots \\ x_n(t) \end{bmatrix} = \begin{bmatrix} 0 & 1 & \cdots & 0 \\ 0 & 0 & \cdots & 0 \\ & & \ddots & \\ -a_0 & -a_1 & \cdots & -a_{n-1} \end{bmatrix} \begin{bmatrix} x_1(t) \\ x_2(t) \\ \vdots \\ x_n(t) \end{bmatrix} + \begin{bmatrix} 0 \\ 0 \\ \vdots \\ 1 \end{bmatrix} u(t), \tag{2}$$

$$y(t) = \begin{bmatrix} b_0 & b_1 & \cdots & b_m & 0 & \cdots & 0 \end{bmatrix} \begin{bmatrix} x_1(t) \\ x_2(t) \\ \vdots \\ x_n(t) \end{bmatrix}. \tag{3}$$

Since each state variable is in a differential relation from the state equation (2), the convolution of the output equation (3) in the time domain gives the state trajectory $\boldsymbol{x}_d(t) = \begin{bmatrix} x_{1d}(t) & x_{2d}(t) & \cdots & x_{nd}(t) \end{bmatrix}^\mathsf{T}$ from the output trajectory $y_d(t)$ as

$$x_{1d}(t) = \mathcal{L}^{-1}\left[\frac{1}{b_m s^{m-1} + \cdots + b_1 s + b_0} y_d(s)\right] \tag{4}$$

where $\mathcal{L}^{-1}$ is the inverse Laplace transform.

2) State Trajectory Generation for Multi-Input Multi-Output System: The proposed method of generating the state trajectory from the output trajectory in the MIMO system will be described below.

This proposed method is calculated by the following 6 steps.

1) Laplace transform state equation and output equation
2) Using the singular value decomposition for $\boldsymbol{B}$ matrix
3) Divide the state equation into two parts ($\boldsymbol{W}_u(s)$ and $\boldsymbol{W}_l(s)$) with and without input $\boldsymbol{u}(s)$
4) Concatenate output equations and $\boldsymbol{W}_l(s)$ vertically
5) Solve about state trajectory $\boldsymbol{x}(s)$
6) Calculate $\boldsymbol{x}(t)$ from inverse Laplace transform

The details of each step are explained below.

In this paper, the plant is assumed that $m < n$, $\mathrm{rank}(\boldsymbol{B}) = m$, and does not have the continuous unstable zeros.

The state equation and the output equation of m input m output nth order plant are given by

$$\dot{\boldsymbol{x}}(t) = \boldsymbol{A}\boldsymbol{x}(t) + \boldsymbol{B}\boldsymbol{u}(t), \tag{5}$$

$$\boldsymbol{y}(t) = \boldsymbol{C}\boldsymbol{x}(t), \tag{6}$$

where the state variables $\boldsymbol{x}(t) \in \mathbb{R}^{n\times 1}$, the input $\boldsymbol{u}(t) \in \mathbb{R}^{m\times 1}$, the output $\boldsymbol{y}(t) \in \mathbb{R}^{m\times 1}$, and the matrices $\boldsymbol{A} \in \mathbb{R}^{n\times n}$, $\boldsymbol{B} \in \mathbb{R}^{n\times m}$, and $\boldsymbol{C} \in \mathbb{R}^{m\times n}$.

The singular value decomposition of the matrix $\boldsymbol{B}$ is given by

$$\boldsymbol{B} = \boldsymbol{U}\boldsymbol{\Sigma}\boldsymbol{V}^*, \tag{7}$$

where $\boldsymbol{U} \in \mathbb{R}^{n\times n}$, $\boldsymbol{\Sigma} \in \mathbb{R}^{n\times m}$, $\boldsymbol{V} \in \mathbb{R}^{m\times m}$.

The elements of $\boldsymbol{\Sigma}$ are given by

$$\begin{aligned}\boldsymbol{\Sigma} &= \begin{bmatrix}\boldsymbol{\Delta}\\ \boldsymbol{O}\end{bmatrix}\\ \boldsymbol{\Delta} &= \mathrm{diag}(\sigma_i)\,(i = 1\cdots m \in \mathbb{N}),\end{aligned}$$

where $\sigma_i\,(i = 1, 2, \ldots, m \in \mathbb{N})$ are the singular values of the matrix $\boldsymbol{B}$.

Multiply both sides of (7) by $\boldsymbol{U}^{-1}$ from the left

$$\begin{aligned}\boldsymbol{U}^{-1}\boldsymbol{B} &= \boldsymbol{\Sigma}\boldsymbol{V}^*\\ &= \begin{bmatrix}\boldsymbol{\Delta}\boldsymbol{V}^*\\ \boldsymbol{O}\end{bmatrix}.\end{aligned} \tag{8}$$

Laplace transform of the state equation (5) is given by

$$s\boldsymbol{x}(s) = \boldsymbol{A}\boldsymbol{x}(s) + \boldsymbol{B}\boldsymbol{u}(s). \tag{9}$$

The state variable conversion of (9) using the transformation matrix $\boldsymbol{U}^{-1}$ as $\tilde{\boldsymbol{x}}(s) = \boldsymbol{U}^{-1}\boldsymbol{x}(s)$ is given by

$$\begin{aligned}&s(\boldsymbol{U}^{-1}\boldsymbol{x}(s)) = (\boldsymbol{U}^{-1}\boldsymbol{A}\boldsymbol{U})(\boldsymbol{U}^{-1}\boldsymbol{x}(s)) + (\boldsymbol{U}^{-1}\boldsymbol{B})\boldsymbol{u}(s)\\ &\Leftrightarrow (s\boldsymbol{I} - \boldsymbol{U}^{-1}\boldsymbol{A}\boldsymbol{U})\tilde{\boldsymbol{x}}(s) = (\boldsymbol{U}^{-1}\boldsymbol{B})\boldsymbol{u}(s)\\ &\Leftrightarrow \boldsymbol{W}(s)\tilde{\boldsymbol{x}}(s) = \begin{bmatrix}\boldsymbol{\Delta}\boldsymbol{V}^*\\ \boldsymbol{O}\end{bmatrix}\boldsymbol{u}(s).\end{aligned} \tag{10}$$

$\boldsymbol{W}(s)$ of (10) is represented as

$$\boldsymbol{W}(s) = \begin{bmatrix}\boldsymbol{W}_u(s)\\ \boldsymbol{W}_l(s)\end{bmatrix}, \tag{11}$$

where $\boldsymbol{W}(s) = s\boldsymbol{I} - \boldsymbol{U}^{-1}\boldsymbol{A}\boldsymbol{U}$, $\boldsymbol{W}_u(s) \in \mathbb{C}^{m\times n}$, and $\boldsymbol{W}_l(s) \in \mathbb{C}^{(n-m)\times n}$.

From (10) and (11)

$$\begin{bmatrix}\boldsymbol{W}_u(s)\\ \boldsymbol{W}_l(s)\end{bmatrix}\tilde{\boldsymbol{x}}(s) = \begin{bmatrix}\boldsymbol{\Delta}\boldsymbol{V}^*\\ \boldsymbol{O}\end{bmatrix}\boldsymbol{u}(s). \tag{12}$$

The extracted lower $(n - m)$ rows of (12) is given by

$$\boldsymbol{W}_l(s)\tilde{\boldsymbol{x}}(s) = \boldsymbol{O}. \tag{13}$$

Laplace transform of the output equation (6) is given by

$$\boldsymbol{y}(s) = \boldsymbol{C}\boldsymbol{x}(s). \tag{14}$$

The state variable conversion of (14) using the transformation matrix $\boldsymbol{U}^{-1}$ as $\tilde{\boldsymbol{x}}(s) = \boldsymbol{U}^{-1}\boldsymbol{x}(s)$ is given by

$$\begin{aligned}&\boldsymbol{y}(s) = (\boldsymbol{C}\boldsymbol{U})(\boldsymbol{U}^{-1}\boldsymbol{x}(s))\\ &\Leftrightarrow (\boldsymbol{C}\boldsymbol{U})\tilde{\boldsymbol{x}}(s) = \boldsymbol{y}(s).\end{aligned} \tag{15}$$

The concatenate matrix from (13) and (15) is given by

$$\begin{bmatrix}\boldsymbol{C}\boldsymbol{U}\\ \boldsymbol{W}_l(s)\end{bmatrix}\tilde{\boldsymbol{x}}(s) = \begin{bmatrix}\boldsymbol{y}(s)\\ \boldsymbol{O}\end{bmatrix}. \tag{16}$$

From (16), the state trajectory $\tilde{\boldsymbol{x}}(s)$ from the output trajectory $\boldsymbol{y}(s)$ in the MIMO system is given by

$$\tilde{\boldsymbol{x}}(s) = \begin{bmatrix}\boldsymbol{C}\boldsymbol{U}\\ \boldsymbol{W}_l(s)\end{bmatrix}^{-1}\begin{bmatrix}\boldsymbol{y}(s)\\ \boldsymbol{O}\end{bmatrix}. \tag{17}$$

From the state variable conversion of (17) using the transformation matrix $\boldsymbol{U}$ as $\boldsymbol{x}(s) = \boldsymbol{U}\tilde{\boldsymbol{x}}(s)$, the state trajectory $\boldsymbol{x}(s)$ from the output trajectory $\boldsymbol{y}(s)$ in the MIMO system is given by

$$\begin{aligned}(\boldsymbol{U}\tilde{\boldsymbol{x}}(s)) &= \boldsymbol{U}\begin{bmatrix}\boldsymbol{C}\boldsymbol{U}\\ \boldsymbol{W}_l(s)\end{bmatrix}^{-1}\begin{bmatrix}\boldsymbol{y}(s)\\ \boldsymbol{O}\end{bmatrix}\\ \Leftrightarrow \boldsymbol{x}(s) &= \boldsymbol{U}\begin{bmatrix}\boldsymbol{C}\boldsymbol{U}\\ \boldsymbol{W}_l(s)\end{bmatrix}^{-1}\begin{bmatrix}\boldsymbol{y}(s)\\ \boldsymbol{O}\end{bmatrix}.\end{aligned} \tag{18}$$

By inverse Laplace transform of (18), the state trajectory $\boldsymbol{x}_d(t)$ from the output trajectory $\boldsymbol{y}_d(t)$ in the MIMO system is given by

$$\boldsymbol{x}_d(t) = \mathcal{L}^{-1}\left[\boldsymbol{U}\begin{bmatrix}\boldsymbol{C}\boldsymbol{U}\\ \boldsymbol{W}_l(s)\end{bmatrix}^{-1}\begin{bmatrix}\boldsymbol{y}_d(s)\\ \boldsymbol{O}\end{bmatrix}\right]. \tag{19}$$

B. Multirate Feedforward

1) Multirate Feedforward for Single-Input Single-Output System: Multirate feedforward control can achieve PTC [1]. A digital tracking control system usually has two samplers for the reference signal $r(t)$ and the output $y(t)$, and one holder on the input $u(t)$, as shown in Fig. 2. Therefore, there exist three time periods T_r, T_y, and T_u which represent the periods of $r(t)$, $y(t)$, and $u(t)$, respectively, as shown in Fig. 3. Additionally, the longer period of T_r and T_y is defined as the frame period T_f. In the case of the SISO nth order plant, $T_r = nT_y = nT_u = T_f$.

Consider the continuous-time nth order plant described by the state equation (20) and the output equation (21).

$$\dot{\boldsymbol{x}}(t) = \boldsymbol{A}_c\boldsymbol{x}(t) + \boldsymbol{b}_c\boldsymbol{u}(t) \tag{20}$$

$$y(t) = \boldsymbol{c}_c\boldsymbol{x}(t) \tag{21}$$

From discretization of (20) and (21) by zero order hold in sampling period T_u, the discrete-time plant becomes the state equation (22) and output equation (23).

$$\boldsymbol{x}[k+1] = \boldsymbol{A}_s\boldsymbol{x}[k] + \boldsymbol{b}_s u[k] \tag{22}$$

$$y[k] = \boldsymbol{c}_s\boldsymbol{x}[k] \tag{23}$$

where the matrices $\boldsymbol{A}_s$, $\boldsymbol{b}_s$, and $\boldsymbol{c}_s$ are given by

$$\boldsymbol{A}_s = e^{\boldsymbol{A}_c T_u}, \tag{24}$$

$$\boldsymbol{b}_s = \int_0^{T_u} e^{\boldsymbol{A}_c\tau}\boldsymbol{b}_c d\tau, \tag{25}$$

$$\boldsymbol{c}_s = \boldsymbol{c}_c. \tag{26}$$

By lifting the discrete-time state equation (22) and the output equation (23), the state equation (27) and the output equation (28) are given by

$$\boldsymbol{x}[i+1] = \boldsymbol{A}\boldsymbol{x}[i] + \boldsymbol{B}\boldsymbol{u}[i], \tag{27}$$

$$y[i] = \boldsymbol{c}\boldsymbol{x}[i], \tag{28}$$

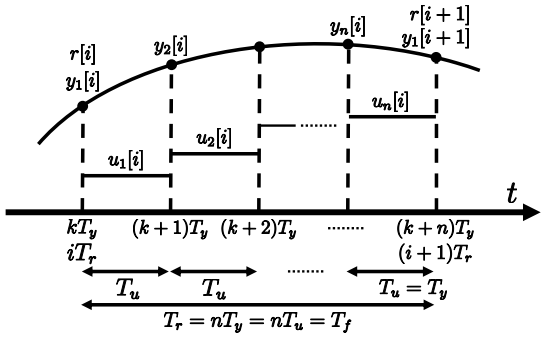

Fig. 3. Multirate sampling control at same interval.

where the matrices $\boldsymbol{A}$, $\boldsymbol{B}$, and $\boldsymbol{c}$, and i are given by

$$\boldsymbol{A} = \boldsymbol{A}_s^n, \tag{29}$$

$$\boldsymbol{B} = \begin{bmatrix} \boldsymbol{A}_s^{n-1}\boldsymbol{b}_s & \boldsymbol{A}_s^{n-2}\boldsymbol{b}_s & \cdots & \boldsymbol{A}_s\boldsymbol{b}_s & \boldsymbol{b}_s \end{bmatrix}, \tag{30}$$

$$\boldsymbol{c} = \boldsymbol{c}_s, \tag{31}$$

$$\boldsymbol{x}[i] = \boldsymbol{x}(iT_r). \tag{32}$$

(27) and (28) are given from the interval between $t = iT_r = kT_u$ and $t = (i+1)T_r = (k+n)T_u$. Input and output vectors $\boldsymbol{u}[i]$ (33) and $\boldsymbol{y}[i]$ (34) are given by

$$\begin{aligned} \boldsymbol{u}[i] &= \begin{bmatrix} u_1[i] & u_2[i] & \cdots & u_n[i] \end{bmatrix}^\mathsf{T} \\ &= \begin{bmatrix} u(kT_u) & u((k+1)T_u) & \cdots & u((k+n-1)T_u) \end{bmatrix}^\mathsf{T}, \end{aligned} \tag{33}$$

$$\begin{aligned} \boldsymbol{y}[i] &= \begin{bmatrix} y_1[i] & y_2[i] & \cdots & y_n[i] \end{bmatrix}^\mathsf{T} \\ &= \begin{bmatrix} y(kT_y) & y((k+1)T_y) & \cdots & y((k+n-1)T_y) \end{bmatrix}^\mathsf{T}. \end{aligned} \tag{34}$$

From (27), the control input $\boldsymbol{u}_{ff}[i]$ to achieve PTC are given by

$$\boldsymbol{u}_{ff}[i] = \boldsymbol{B}^{-1}(\boldsymbol{I} - z^{-1}\boldsymbol{A})\boldsymbol{x}[i+1]. \tag{35}$$

The block diagram of the control system is shown in Fig. 2. L is a discrete-time lifting operator [11]. L^{-1} outputs the elements of nth dimensional vector $\boldsymbol{u}_{ff}[i]$, which is input every period T_r, in order from 1 to n by $T_u = T_r/n$.

2) Multirate Feedforward for Multi-Input Multi-Output System: In m-input p-output nth order MIMO system, the state equation (36) and the output equation (37) of the continuous-time plant are given by

$$\dot{\boldsymbol{x}}(t) = \boldsymbol{A}_c\boldsymbol{x}(t) + \boldsymbol{B}_c\boldsymbol{u}(t) \tag{36}$$

$$\boldsymbol{y}(t) = \boldsymbol{C}_c\boldsymbol{x}(t) \tag{37}$$

$$\boldsymbol{B}_c = \begin{bmatrix} \boldsymbol{b}_{c1} & \cdots & \boldsymbol{b}_{cm} \end{bmatrix} \tag{38}$$

$$\boldsymbol{C}_c = \begin{bmatrix} \boldsymbol{c}_{c1} & \cdots & \boldsymbol{c}_{cp} \end{bmatrix}^\mathsf{T} \tag{39}$$

where the plant state $\boldsymbol{x} \in \mathbb{R}^n$, the plant input $\boldsymbol{u} \in \mathbb{R}^m$, and the plant output $\boldsymbol{u} \in \mathbb{R}^p$.

Generalized controllability indices are defined as follows [7].

Definition (Generalized Controllability Indices)**.** *Generalized controllability indices of $(\boldsymbol{A}_c, \boldsymbol{B}_c)$ are defined as follows for $\boldsymbol{A}_c \in \mathbb{R}^{n\times n}$ and $\boldsymbol{B}_c = [\boldsymbol{b}_{c1}, \cdots, \boldsymbol{b}_{cm}] \in \mathbb{R}^{n\times m}$. If $(\boldsymbol{A}_c, \boldsymbol{B}_c)$ is a controllable pair, n linearly independent vectors can be selected from*

$$\{\boldsymbol{b}_{c1}, \cdots, \boldsymbol{b}_{cm}, \boldsymbol{A}_c\boldsymbol{b}_{c1}, \cdots, \boldsymbol{A}_c\boldsymbol{b}_{cm}, \cdots, \boldsymbol{A}_c^{n-1}\boldsymbol{b}_{cm}\}.$$

Letting φ be a set of these n vectors, σ_l, and N are defined by

$$\sigma_l = \text{number}\{k | \boldsymbol{A}_c^{k-1}\boldsymbol{b}_{cl} \in \varphi\}, \tag{40}$$

$$\sum_{l=1}^{m} \sigma_l = n, \tag{41}$$

$$N = \max(\sigma_l). \tag{42}$$

In the case of MIMO system, $n\,(=\text{plant order})$ number of vectors are selected from generalized controllability indices, and the full row rank matrix $\boldsymbol{B}$ are designed. Therefore, the feedforward controllers have different forms according to their choice.

From (43), the control input $\boldsymbol{u}_{ff}[i]$ to achieve PTC are given by (44).

$$\boldsymbol{x}[i+1] = \boldsymbol{A}\boldsymbol{x}[i] + \boldsymbol{B}\boldsymbol{u}[i], \tag{43}$$

$$\boldsymbol{u}_{ff}[i] = \boldsymbol{B}^{-1}(\boldsymbol{I} - z^{-1}\boldsymbol{A})\boldsymbol{x}[i+1], \tag{44}$$

where the matrices $\boldsymbol{A}$, $\boldsymbol{x}[i]$, $\boldsymbol{u}[i]$, and z are given by

$$\boldsymbol{A} = e^{\boldsymbol{A}_c T_f}, \tag{45}$$

$$\boldsymbol{x}[i] = \boldsymbol{x}(iT_f), \tag{46}$$

$$\begin{aligned} \boldsymbol{u}[i] &= \begin{bmatrix} \boldsymbol{u}_1[i] & \cdots & \boldsymbol{u}_m[i] \end{bmatrix}^\mathsf{T} \\ &= \begin{bmatrix} u_{11}[i] & \cdots & u_{1\sigma_1}[i] & u_{21}[i] & \cdots & u_{m\sigma_m}[i] \end{bmatrix}^\mathsf{T}, \end{aligned} \tag{47}$$

$$z = e^{sT_f}, \tag{48}$$

$$T_f = NT_u. \tag{49}$$

III. Experiment

A. Modeling

In the simulation and experiment, the authors control the fine stage of the 6 DOF high-precision stage shown in Fig. 1(a). This fine stage is supported by 6 DOF air bearing gravity canceller. In this paper, controlling 2 DOF of the translation x along the x axis and the pitching θ_y around and y axis, as shown in Fig. 1(b).

The equations of motion of the translation and pitching of the stage are given by (50) and (51) [5].

$$(M_{x1} + M_{x2})\ddot{x}_{g1} + C_{x1}\dot{x}_{g1} + K_{x1}x_{g1} + M_{x2}L_{g2}\ddot{\theta}_y = f_x \tag{50}$$

$$(M_{x2}L_{g2}^2 + J_{\theta y})\ddot{\theta}_y + C_{\theta y}\dot{\theta}_y + K_{\theta y}\theta_y + M_{x2}L_{g2}(\ddot{x}_{g1} - g\theta_y) = \tau_y + f_x L_{fx} \tag{51}$$

Convert x_{g1} to observable x_m by (52).

$$x_m(s) = x_{g1}(s) + L_m\theta_y(s) \tag{52}$$

From (50), (51), and (52), transfer functions g_{11} to g_{22} in Fig. 1(c) are given. In the proposed method, this plant model is represented in the balanced realization.

The parameters of the stage are shown in Table I, which is given from fitting in the frequency domain, shown in Fig. 4.

TABLE I
MODEL PARAMETERS.

Symbol	Meaning	Value
x_m	Measured position of the fine stage	–
x_{g1}	Position of the CoG of the planar air bearing and the air gyro	–
x_{g2}	Position of the CoG of the fine stage	–
θ_y	Measured attitude angle of the fine stage	–
f_x	Input force of the fine stage in the x direction	–
τ_y	Input torque of the fine stage in the θ_y direction	–
M_{x1}	Mass of the planar air bearing and the air gyro	0.077 kg
C_{x1}	Viscosity coefficient in the x_{g1} motion	200 N/(m/s)
K_{x1}	Spring coefficient in the x_{g1} motion	5000 N/m
M_{x2}	Mass of the fine stage	5.3 kg
$J_{\theta y}$	Moment of inertia of the fine stage	0.10 kgm^2
$C_{\theta y}$	Viscosity coefficient of the fine stage in the θ_y motion	1.6 Nm/(rad/s)
$K_{\theta y}$	Spring coefficient of the fine stage in the θ_y motion	1200 Nm/rad
L_m	Distance between the measurement point of x_m and the CoR	-0.028 m
L_{g2}	Distance between the CoR and the CoG of the fine stage	-0.051 m
L_{fx}	Distance between the CoR of the fine stage and the actuation point	-0.0026 m

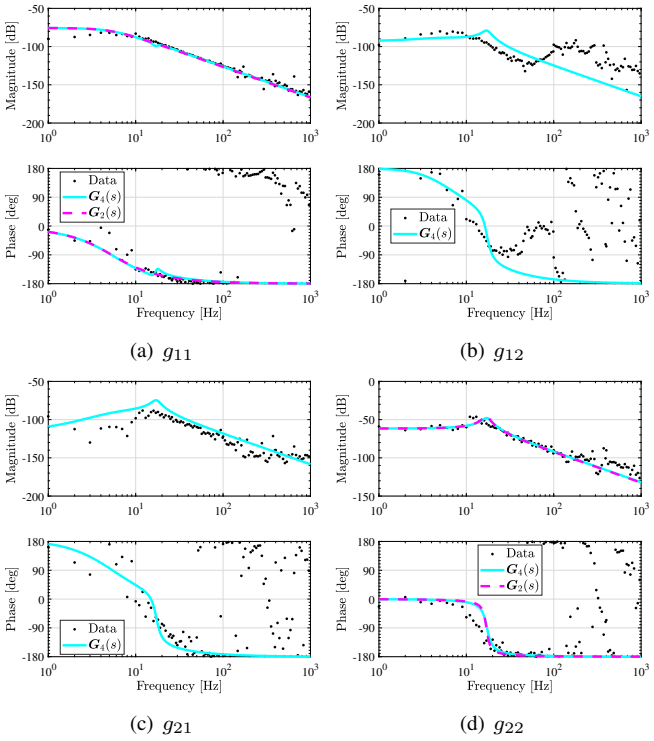

(a) g_{11} (b) g_{12} (c) g_{21} (d) g_{22}

Fig. 4. Frequency responses of the plant. $\boldsymbol{G}_4$ and $\boldsymbol{G}_2$ denote a 4th order MIMO nominal plant and a 2nd order SISO nominal plant, respectively.

B. Conditions

The block diagram of the simulation is shown in Fig. 2. Generally, a dual-input dual-output plant with the interference is represented by a block diagram as shown in Fig. 1(c). g_{11} to g_{22} represent the transfer function of each path.

Conventional method 1 ignores the interference by g_{12} and g_{21} and the multirate feedforward controllers are designed for each SISO system g_{11} and g_{22}, respectively, as shown in Fig. 5(a). Coupling is suppressed by the feedback controller.

Conventional method 2 designs a precompensator for continuous-time plants that cancels the interference between axes by g_{12} and g_{21}, and the multirate feedforward controllers are designed for each decoupled SISO system g_{11} and g_{22}, respectively, as shown in Fig. 5(b). In this method, the precompensator is discretized by the bilinear transformation. Since the problem of the unstable discretization zero is not considered, PTC cannot theoretically be achieved.

In the proposed method, a dual-input dual-output multirate feedforward controller is designed for a dual-input dual-output plant as shown in Fig. 5(c).In this paper, the selection of the generalized controllability indices in the proposed method $(\sigma_1, \sigma_2) = (2, 2)$ is given by

$$\boldsymbol{B} = \begin{bmatrix} \boldsymbol{A}_s \boldsymbol{b}_{s1} & \boldsymbol{b}_{s1} & \boldsymbol{A}_s \boldsymbol{b}_{s2} & \boldsymbol{b}_{s2} \end{bmatrix} \tag{53}$$

In Fig. 4, $\boldsymbol{G}_4$ is used for MIMO plant model of the proposed method, and $\boldsymbol{G}_2$ is used for SISO plant model of the conventional method 1 and 2.

In the simulation, the feedback controller $\boldsymbol{C}_{fb}[z_s]$ is 0 in the all methods. In the experiment, $\boldsymbol{C}_{fb}[z_s]$ are PID controllers tuned to have 20 Hz closed roop pole for all 6 DOF $(x, y, z, \theta_x, \theta_y, \theta_z)$ in the all methods.

7th order polynomial trajectory of 0 µm to 100 µm in 0 ms to 20 ms is given for x_m^{ref} and 7th order polynomial trajectory of 0 µrad to 100 µrad in 0 ms to 20 ms is given for θ_y^{ref}. $T_u = 200$ µs, $N = \max(\sigma_1, \sigma_2)$, and $T_r = NT_y = NT_u = T_f$.

C. Simulation Results

The simulation results are shown in Fig. 6. From the simulation results, PTC cannot be achieved with the conventional method, but it can be achieved in the proposed method. The effectiveness of the proposed method is verified.

D. Experiment Results

In the experiment, the proposed method of $(\sigma_1, \sigma_2) = (2, 2)$, the conventional method 1, and the conventional method 2 are compared under the same conditions as the simulation.

The experiment result is shown in Fig. 7. From the experiment results, the tracking errors of x_m are close values in all methods. The tracking errors of x_m in the conventional method 2 and the proposed method become bigger than the simulation results due to the effect of modeling error, shown in Fig. 4. However, the tracking error of θ_y in the proposed method is the smallest compared with those of the conventional methods. The effectiveness of the proposed method is verified.

IV. CONCLUSION

In this paper, the authors propose the multirate feedforward controller and the generating method of the state trajectory corresponding to the output trajectory for MIMO systems. In the MIMO multirate feedforward controller design, the authors show that several kinds of controllers can be designed for the $\boldsymbol{B}$ matrix selected from the generalized controllability indices. In addition, the authors show the generating method of the state trajectory in any state space representation using singular value decomposition. The effectiveness of the proposed method is verified by simulations and experiments in translation and pitching motions of the 6 DOF high-precision stage. The case in which the plant has continuous unstable zeros and the extension from 2 DOF to 6 DOF are future work.

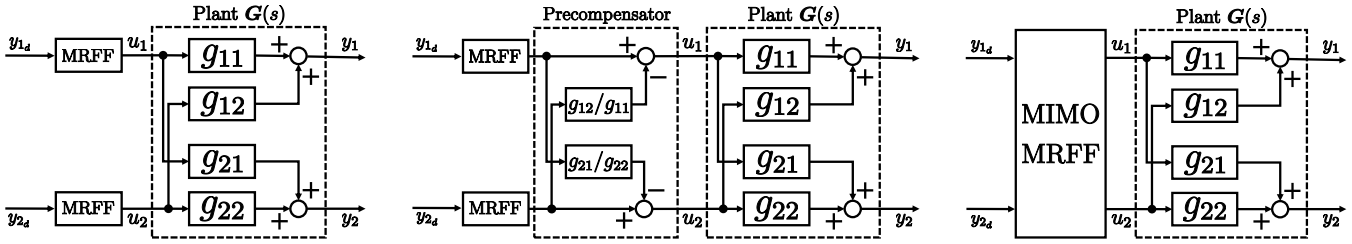

(a) Conventional method 1. (b) Conventional method 2. (c) Proposed method.

Fig. 5. Block diagram of the control methods. These show only feedforward controllers.

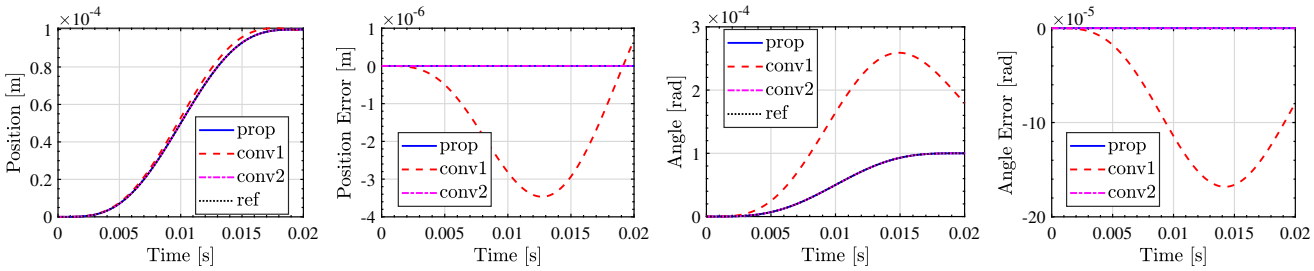

(a) x_m (b) e_{x_m} (c) θ_y (d) e_{θ_y}

Fig. 6. Simulation results.

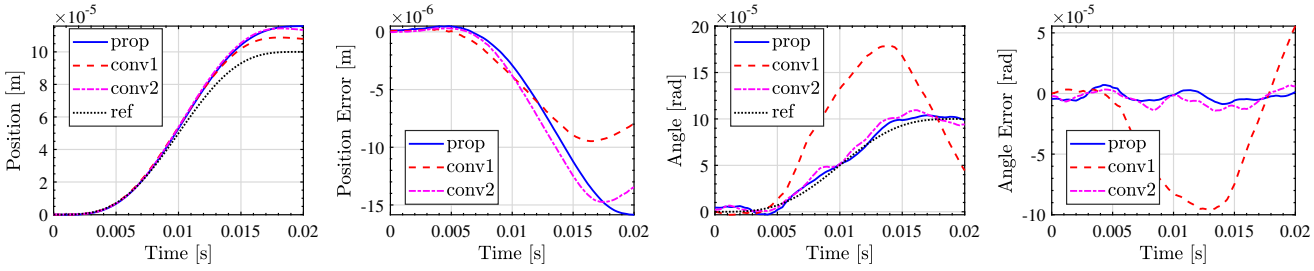

(a) x_m (b) e_{x_m} (c) θ_y (d) e_{θ_y}

Fig. 7. Experimental results.

REFERENCES

[1] H. Fujimoto, Y. Hori, and A. Kawamura, "Perfect tracking control based on multirate feedforward control with generalized sampling periods," *IEEE Transactions on Industrial Electronics*, vol. 48, no. 3, pp. 636–644, jun 2001.

[2] M. Tomizuka, "Zero Phase Error Tracking Algorithm for Digital Control," *Journal of Dynamic Systems, Measurement, and Control*, vol. 109, no. 1, p. 65, 1987.

[3] T. Oomen, "Advanced Motion Control for Precision Mechatronics: Control, Identification, and Learning of Complex Systems," *IEEJ Journal of Industry Applications*, vol. 7, no. 2, pp. 127–140, 2018.

[4] G. E. Moore, "Cramming More Components Onto Integrated Circuits," *Electronics*, vol. 38, no. 8, 1965.

[5] W. Ohnishi, H. Fujimoto, K. Sakata, K. Suzuki, and K. Saiki, "Decoupling Control Method for High-Precision Stages using Multiple Actuators considering the Misalignment among the Actuation Point, Center of Gravity, and Center of Rotation," *IEEJ Journal of Industry Applications*, vol. 5, no. 2, pp. 141–147, 2016.

[6] H. Butler, "Position Control in Lithographic Equipment," *IEEE Control Systems*, vol. 31, no. 5, pp. 28–47, oct 2011.

[7] H. Fujimoto, "General Framework of Multirate Sampling Control and Applications to Motion Control Systems," Ph.D. dissertation, 2000.

[8] M. Mae, W. Ohnishi, H. Fujimoto, and Y. Hori, "Perfect Tracking Control of Dual-Input Dual-Output System for High-Precision Stage in Translation and Pitching Motion," *Proceedings of the International Workshop on Sensing, Actuation, Motion Control, and Optimization*, no. 5, pp. TT6–5, 2018.

[9] W. Ohnishi, T. Beauduin, and H. Fujimoto, "Preactuated multirate feedforward for a high-precision stage with continuous time unstable zeros," *IFAC-PapersOnLine*, vol. 50, no. 1, pp. 10 907–10 912, jul 2017.

[10] J. van Zundert, J. Bolder, S. Koekebakker, and T. Oomen, "Resource-efficient ILC for LTI/LTV systems through LQ tracking and stable inversion: Enabling large feedforward tasks on a position-dependent printer," *Mechatronics*, vol. 38, pp. 76–90, 2016.

[11] T. Chen and B. A. Francis, *Optimal Sampled-Data Control Systems*. London: Springer London, 1995.